SEISMICA

Along-strike changes in ETS behavior near the slab edge of Southern Cascadia

C.P. Nuyen 🆔 *[1], D.A. Schmidt 🆔[1]

[1]Department of Earth and Space Sciences, University of Washington, Seattle, USA

Author contributions: *Conceptualization*: C.P. Nuyen, D.A. Schmidt. *Formal Analysis*: C.P. Nuyen. *Methodology*: C.P. Nuyen, D.A. Schmidt. *Supervision*: D.A. Schmidt. *Writing – original draft*: C.P. Nuyen. *Writing – review & editing*: C.P. Nuyen, D.A. Schmidt.

Abstract   Episodic tremor and slip (ETS) is well-documented along the entire length of the Cascadia subduction zone. We explore how the occurrence of ETS varies at the southernmost edge of the subduction zone, where geometric complexity and a slab window likely alter conditions along the plate interface. This work uses tremor and GNSS time series data to identify nineteen of the largest ETS events in southern Cascadia between 2016.5-2022 and document source properties for events approaching the slab edge. Distributed slip models for these events show that cumulative fault slip along the megathrust reaches a maximum near 40.5° N latitude and that large ETS events accommodate up to 85% of plate convergence at this location. However, ETS fault slip and tremor terminate near 40° N latitude, some 50 km before the southern lateral edge of the subducting plate. After considering a range of explanations, we propose that the complex geometry and progressive heating of the subducting plate modifies ETS behavior and does not allow seismic slip to occur along the plate interface in southernmost Cascadia below 35 km depth.

Non-technical summary   In subduction zones, there is a deep zone along the plate boundary where the two plates periodically slip past each other during slow earthquakes. These slow earthquakes can be accompanied by a seismic phenomenon known as tremor, and together these events are known as episodic tremor and slip (ETS). Although ground shaking is greatly diminished, ETS events can release the same amount of energy as a Mw 7 earthquake. Studying the location and frequency of ETS events is important for understanding the seismic cycle, since ETS events can impact the timing of larger earthquakes. In this work, we use GNSS and seismic data to identify and characterize ETS events near the southern edge of the Cascadia subduction zone, which is located at the junction of three tectonic plates. Results from this work suggest that ETS does not occur near the southernmost edge of the subduction zone. We hypothesize that structural complexities and elevated temperatures in this region prohibit ETS from occurring at typical depths along the plate boundary. These findings are important, as they help illuminate the non-uniformity of ETS behavior in Cascadia and illustrate what factors may be influencing ETS in subduction zones.

1   Introduction

In subduction zone systems, interseismic strain along the plate interface is periodically released at certain depths by slow slip events (SSEs; Schwartz and Rokosky, 2007). These events typically occur along the plate boundary downdip of the seismogenic locked zone and updip of the creeping portion of the fault (Ito et al., 2007). SSEs involve a component of accelerated aseismic slip along the plate interface and manifest as transient surface displacements in GNSS time series data (Rogers and Dragert, 2003). These events are also associated with seismic shear slip along the plate interface, which produces non-volcanic tremor and low-frequency earthquakes (LFEs) that coincide spatially and temporally with the SSEs (Ide et al., 2007; Shelly et al., 2007). Together, these periodic seismic and aseismic phenomena are termed episodic tremor and slip (ETS).

Ample work has been done to study ETS in the Cascadia subduction zone (Gomberg, 2010), with margin-wide studies providing insights on the broad patterns of tremor and slow slip along the margin (e.g. Bartlow, 2020) and more localized studies shedding light on the characteristics of individual events, such as moment magnitude and fault slip amplitude (e.g. Schmidt and Gao, 2010). However, only a small portion of this work has focused exclusively on southern Cascadia, where ETS encounters the southern edge of the subduction zone (Figure 1). Although several studies analyze the characteristics of individual ETS events in this region, such as slip amplitudes on the megathrust and tremor migration patterns (Schmalzle et al., 2014; McKenzie et al., 2020; Boyarko and Brudzinski, 2010), the various methods and *a priori* assumptions used by these studies make it difficult to directly compare their results and discern if the behavior of ETS events changes along-strike or near the edge of the subduction zone.

This study examines nineteen of the largest SSEs in Southern Cascadia from mid 2016 to 2022. Using tremor and GNSS time series data, we determine the timing

---

*Corresponding author: Carolyn Nuyen (cnuyen@uw.edu)
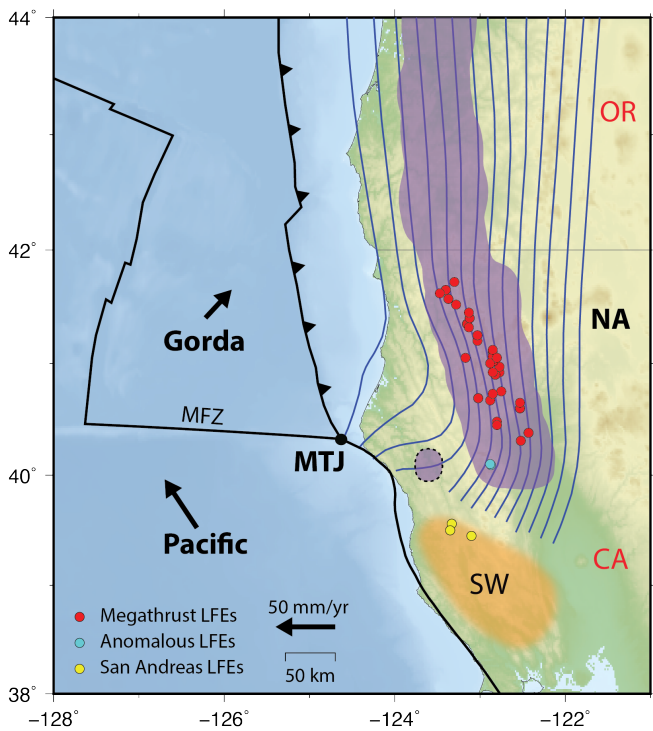
Figure 1 Map of the southern Cascadia subduction zone. Black arrows show plate motion relative to North America (NA), blue lines delineate slab depth contours from Mc-Crory et al. (2012) every 5 km starting at 15 km depth, purple polygon shows the outline of tremor locations from the Pacific Northwest Seismic Network tremor catalog (https://pnsn.org/tremor) with the updip tremor patch from Wech (2021) outlined with a dashed black line. Yellow and red circles show the location of LFE families associated with the San Andreas fault system and megathrust, respectively (Plourde et al., 2015; Ducellier and Creager, 2022). Overlapping cyan circles show an anomalous pair of LFE families with near-continuous temporal activity. Black circle shows the location of the Mendocino triple junction (MTJ). Orange region shows the location of the inferred slab window (SW). State names (red lettering): OR, Oregon; CA, California. MFZ, Mendocino fracture zone.

and horizontal surface displacements associated with these events, and invert for the slip distribution on the megathrust fault. These slip models allow us to compare patterns of tremor and fault slip between numerous ETS events and analyze how transient strain release is distributed near the southern edge of the subduction zone. Our results show that ETS terminates >50 km north of the Gorda slab edge and suggest that ETS behavior in southernmost Cascadia may be influenced by slab geometry and the presence of an inferred slab window near the triple junction.

2 Background

2.1 Gorda Slab Structure

Southern Cascadia is characterized by the subduction of the Gorda slab beneath the North American plate in southern Oregon and northern California (Figure 1). While the northern portion of the Gorda slab is invari-

ant along strike between 42° and 43° N latitude, the southernmost portion exhibits a convex geometry beneath northern California. Specifically, the slab flattens between 15 and 25 km depth, creating a broad high centered at 41° N latitude (McCrory et al., 2012; Guo et al., 2021). Downdip of 25 km depth, the slab arcs around this shallowly dipping region to create a bend that extends to the edge of the subduction zone. This distortion is attributed to the northward impingement of the Pacific plate on the Gorda slab, which results in the internal deformation of the slab offshore (Chaytor et al., 2004; McCrory et al., 2012; Ismat et al., 2022). Seismic velocity models and the location of earthquake hypocenters in southern Cascadia also suggest that the southernmost edge of the slab is dipping south-to-southeast by 6-12° (Furlong and Schwartz, 2004; Verdonck and Zandt, 1994). This complex slab geometry in southernmost Cascadia likely interacts with mantle flow patterns near the edge of the subduction zone (Schellart, 2004; Bodmer et al., 2018).

Offshore of Cape Mendocino, the southern boundary of the Gorda plate is clearly delineated by the Mendocino fracture zone. However, following subduction, the location of the slab edge becomes less obvious. As a result, the southern terminus of the McCrory et al. (2012) slab model in Figure 1 is inferred from the first-motion readings at seismic stations after the 1994 Mw 7.1 Mendocino earthquake (McCrory et al., 2004). Specifically, McCrory et al. (2004) observe a change in the first-motion recordings at seismic stations in northern California that occurs across a boundary that intersects the coast at the Mendocino triple junction (MTJ) with an azimuth of ~120°. McCrory et al. attribute this first-motion pattern to a seismic wavefront that diffracted into the Gorda slab and interpret this boundary as the slab edge. This slab edge location is also supported by subsurface models that are constrained by gravity data (Jachens and Griscom, 1983).

2.2 Mendocino Triple Junction and Slab Window

Subduction in southern Cascadia ends at the MTJ, where the Pacific, Gorda, and North American plates meet offshore of Cape Mendocino, CA. Over time, the MTJ steadily migrates northward relative to North America, extending the San Andreas transform boundary by shifting the southern limit of subduction to the north (Atwater, 1970). This northward migration of the MTJ promotes the growth of a slab window directly south of the Gorda slab (Atwater, 1970; Dickinson and Snyder, 1979a,b). As this slab window forms, mantle material flows to fill the space that was previously occupied by the Gorda slab. Various 2-D and 3-D models of the MTJ region predict that this process brings warm mantle material closer to the overlying crust, which then cools over time as it equilibrates with the surrounding lithosphere (Goes et al., 1997; Popov et al., 2012; van Wijk, 2001). Heat flow measurements in northern California show a pronounced increase in heat flow from north to south, with maximum heat flow values occurring ~200 km south of the MTJ (Lachenbruch and Sass,

1980). Thermal models that include conductive and/or advective heat transfer between the slab window and North American lithosphere (e.g. Guzofski and Furlong, 2002; Popov et al., 2012) are able to recreate this high heat flow anomaly and suggest that the slab window is actively warming the overlying crust. Generic models for ridge subduction and subsequent slab window generation suggest that this warming can lead to rheological weakening, causing the transition from brittle to ductile deformation to become shallower (Groome and Thorkelson, 2009).

Seismic velocity and thermomechanical models indicate that the northern edge of the slab window abuts the southern edge of the Gorda slab (Benz et al., 1992; Liu et al., 2012; Stanciu and Humphreys, 2021). Therefore, in addition to the continental lithosphere, hot mantle material in the slab window is likely transferring heat to the edge of the descending Gorda slab as well. Goes et al. (1997) present 3-D thermal models for the MTJ region that incorporate the subducting Gorda slab and allow for the thermal structure to be impacted by variations in the slab's age. An inspection of the figure from these models indicates that at 40 km depth, temperatures along the plate interface 20 km north of the slab edge are ~100 °C warmer than temperatures 100 km north of the slab edge. Therefore, this suggests that temperatures along the plate interface at the slab edge at 40 km depth may have increased by more than 100 °C due to heating from mantle material in the adjacent slab window.

2.3 Previous ETS Observations in Southern Cascadia

ETS events occur frequently in southern Cascadia with recurrence intervals of 10 ± 2 months (Szeliga et al., 2004; Brudzinski and Allen, 2007). These events occur along the plate interface at 30-60 km depth and combine to create a continuous band of tremor and transient fault slip that broadly aligns with the depth contours of the warped Gorda slab (Figure 1; Bartlow, 2020; Wech, 2021; Michel et al., 2018). An anomalous near-continuous patch of tremor is also located near the slab edge and offset ≥40 km to the west of the main tremor zone (Figure 1; Wech, 2021). However, the source of this tremor patch is unclear and could be related to slip on a transform fault within the San Andreas Fault system, slip on the plate interface, or transform slip on the edge of the Gorda slab (Wech, 2021).

Distinct LFE families are also observed in northern California and are attributed to slip along the San Andreas fault system and ETS on the megathrust (Figure 1; Plourde et al., 2015). The ETS families exhibit depth-dependent recurrence intervals, with deeper families having shorter recurrence intervals than shallower families (Ducellier and Creager, 2022). This behavior is also observed for LFEs and tremor in northern Cascadia, where smaller, more frequent events tend to occur downdip of larger, less frequent events (Wech and Creager, 2011; Sweet et al., 2019). Wech and Creager (2011) attribute this spatial relationship to changes in fault strength, suggesting that the megathrust weakens

with depth due to decreases in friction. However, this trend does not apply to the southernmost ETS families in northern California (overlapping pair of cyan dots in Figure 1 indicating two LFE families), which exhibit relatively short recurrence intervals (<50 days) despite being located farther updip (Ducellier and Creager, 2022). Therefore, Ducellier and Creager (2022) propose that these families may be located on a crustal fault above the megathrust and are not associated with ETS on the plate interface.

Changes in the slab geometry and thermal gradient at the edge of the subduction zone may impact the behavior of ETS in southern Cascadia. However, assessing possible changes in ETS behavior is challenging without the compilation and direct comparison of numerous events. Boyarko and Brudzinski (2010) analyze the spatiotemporal patterns of tremor in southern Cascadia between 2005-2007 and present observations on event distribution and migration style. However, this work relies on a semiautomated tremor location algorithm that only considers the most active nighttime hour (in terms of tremor) for every day of a given tremor episode. As a result, this work only considers the most active times of tremor and may not capture the full spatial extent of tremor events. Schmalzle et al. (2014) and McKenzie et al. (2020) present distributed slip models for a total of twelve ETS events in southern Cascadia from 2005.5-2011 and 2014-2017, respectively. Although these studies provide valuable insights on fault slip magnitudes and the orientation of strain accumulation along the megathrust, they represent margin-wide studies that do not focus on characterizing ETS in southern Cascadia. Therefore, we identify and calculate distributed slip models for nineteen ETS events in southern Cascadia to determine if ETS behavior changes at the edge of the Cascadia subduction zone.

3 Data and Methods

We utilize a combination of publicly available tremor and GNSS time series data to characterize ETS events in southern Cascadia. The tremor data are sourced from the Pacific Northwest Seismic Network (PNSN) tremor catalog (https://pnsn.org/tremor), and the GNSS time series data are obtained from the Pacific Northwest Geodetic Array (PANGA) at Central Washington University (PANGA, 1996). We use horizontal east and north component GNSS time series data from 137 stations throughout central and southern Cascadia in the NAM14 stable North American reference frame. GNSS time series data capture signals from various tectonic and non-tectonic sources that can obscure the timing of ETS events. This is particularly true in southern Cascadia, where elevated levels of seismicity indicate active deformation in the region (McCrory et al., 2012). Therefore, we process the GNSS time series data to remove unwanted tectonic signals and non-tectonic noise to make the timing of ETS events more clear. We process the data using the following steps:

- We remove outliers (i.e. positions that stray >20 mm from adjacent observations).

- We remove steps that are due to known earthquakes and equipment changes. The timing of steps is determined by GAGE offsets from the Central Washington University (Herring et al., 2016, https://www.unavco.org/data/gps-gnss/derived-products/derived-products.html). We estimate the step offsets by differencing the average position for the 21 days before the event and the average position for the 21 days after the event.

- We remove the annual and biannual seasonal components and detrend the time series data. We assume that the annual and biannual signals are a combination of sine and cosine waves and model the time series data as a linear combination of seasonal, slope, and offset terms. We solve for the coefficients of these terms using a linear least-squares inversion, and then remove the scaled seasonal and slope terms from the GNSS time series data. Additional details on how we estimate the term coefficients can be found in the Supplemental Information.

- We smooth the time series data by applying a seven-day moving average, which helps remove high-frequency (daily) noise. The initiation and cessation phases of ETS events typically produce small daily displacements that can easily be obscured by noise. Therefore, removing high frequency noise helps to elucidate the starting and stopping times of ETS events. This moving average likely extends the event in time; however, our goal here is to bracket the timing of the largest events for further analysis

3.1 Event Timing and Displacements

We identify the general timing of ETS events in southern Cascadia by visually inspecting the spatiotemporal patterns of tremor (Figure 2). When examining the PNSN tremor catalog (https://pnsn.org/tremor), we focus on continuous tremor events where the majority of tremor occurs south of 44° N latitude and the total duration of tremor associated with an individual ETS event is at least 70 hours. Using these criteria, we identify nineteen ETS events in southern Cascadia between 2016.5 and 2022 (Figure 2). The tremor monitoring system for the PNSN was updated in 2017, resulting in more accurate tremor detection in southern Cascadia (Wech, 2021, K.C. Creager, personal communication, 2022). Therefore, aside from two events at the end of 2016, we do not consider any events prior to 2017 given the changes in the tremor detection algorithm and seismic station network at this time (Wech, 2021). After identifying the nineteen events with the tremor data, we then use the GNSS time series data to estimate the timing and offset amplitude of the associated surface displacements.

ETS events in southern Cascadia manifest as westward displacement transients in GNSS time series data (Szeliga et al., 2004). Therefore, we develop a simple algorithm to identify westward displacements in the GNSS east time series data and estimate the timing of ETS events (Figure 3). For each event, the algorithm starts by locating the GNSS stations that are closest to the event tremor in Figure 2. This is accomplished by finding all stations that have at least 100 epicenters of tremor (where an epicenter represents a detection within a five-minute window) within 30 km of the station. For smaller events with less tremor (e.g. Event 16 indicated in Figure 2), we reduce the number of tremor counts to twenty. We assume that these GNSS stations nearest the tremor experience larger transients than stations farther away and thus offer a clearer picture of when surface deformation is occurring. Therefore, we utilize these stations to estimate the timing of transients and refer to them as 'index' stations. For each index station, the algorithm computes a time series of daily displacements from the horizontal east component GNSS time series data. The algorithm then applies a centered 14-day moving sum to the daily displacement time series data and flags all days where the sum falls above a given threshold (Figure 3A, 3B). For this work, we find that a threshold of 0.5 mm westward is large enough to avoid false-detections due to leftover noise in the data and low enough to capture relatively small transients associated with ETS events. The algorithm then establishes transient start and end times by going through the time series data and looking for consecutively flagged days. When the algorithm finds a succession of flagged days, it marks the first flagged day as a transient start date and the last flagged day as a transient end date. We limit our analysis to transients that last at least seven days, so the algorithm ignores any consecutively flagged days that do not span at least a week (Figure 3C). The algorithm also only considers flagged days that fall within two weeks of the beginning or end of the event tremor shown in Figure 2. Once the algorithm has found the timing of transients for all of the index stations, it then assigns every non-index station the timing of the closest index station by latitude. Finally, the algorithm calculates the east and north component horizontal surface displacements for each station by differencing the average position for the seven days before the transient start date and the average position for the seven days after the transient end date. If a station has multiple start and end dates, then the algorithm sums the displacements from the multiple epochs. Smoothing the GNSS time series data in Step 4 runs the risk of dampening the amplitude of ETS transients. Therefore, we calculate the horizontal surface displacements from GNSS time series data that is processed without applying the final smoothing step (Figure 3C).

We manually inspect the results of our algorithm for each ETS event to ensure consistency between the transient times at different stations and to check that the results are compatible with the tremor data. Overall, we find that the algorithm is able to accurately identify transients in the GNSS time series data that align well with the timing of tremor (Figure 4). However, there are several ETS events where the timing of transients at certain stations can be improved by removing or adding index stations. For example, removing an index station can be helpful when the index station's GNSS data is particularly noisy and the transient timing is impacted by non-tectonic signals. Conversely, it can be beneficial to
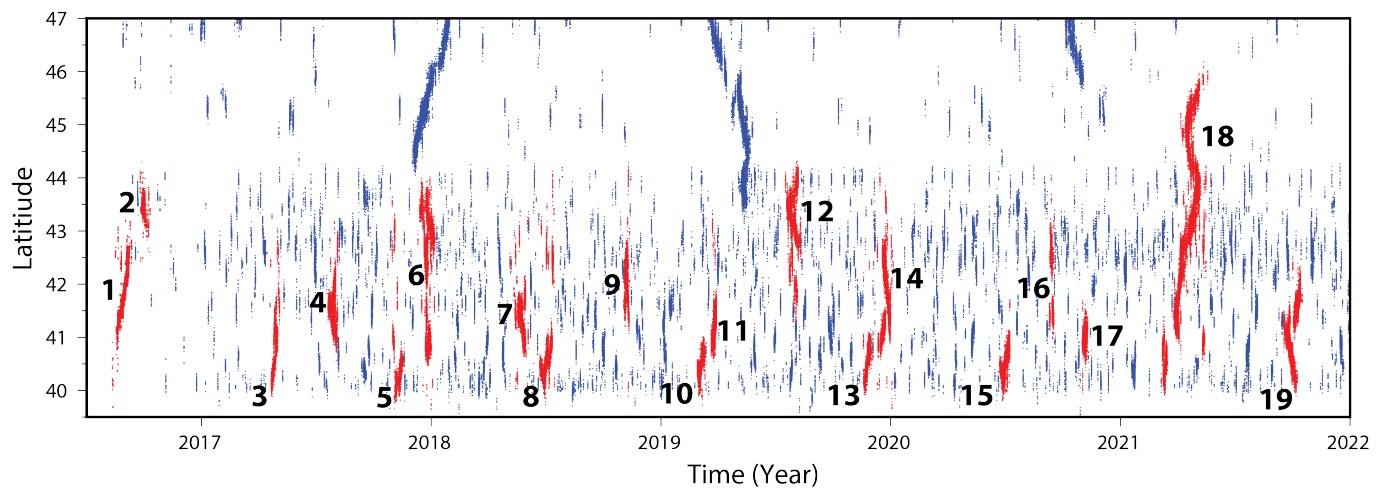
Figure 2 Map of tremor locations in southern Cascadia from the Pacific Northwest Seismic Network tremor catalog (https://pnsn.org/tremor). Red dots show the tremor that is included in the nineteen labeled ETS events. The California-Oregon border is at latitude 42° N.

add index stations when there are clear transients in the GNSS data (Figure 4A). For example, station YBHB consistently shows surface displacements associated with multiple ETS events, but it is not close enough to tremor to be considered an index station. Therefore, we manually remove and/or add index stations for certain ETS events to improve the timing of transient signals in the GNSS time series data. Details for each ETS event, including which index stations are used and the transient start and stop times for each station, can be found in the Supplementary Information.

For ETS Event 9 (November 2018), we observe a large-scale regional pattern of westward surface displacements at GNSS stations throughout Cascadia (Figure S1). The tremor during this event is concentrated on the Oregon-California border and the GNSS stations nearest the tremor exhibit larger westward transients than the surrounding stations. Therefore, we believe that the displacements for this ETS event are over-printed by a widespread common-mode signal. To remove this signal, we average the displacements at all stations located south of 40° N latitude or east of -121° W longitude, since we believe that these stations are far enough away from the event tremor that they should not experience any displacements. This average displacement was then removed from all of the stations to create the final displacement field shown in Figures S1 and S11 (e.g. Dong et al., 2006).

3.2 Inversion

We invert the horizontal surface displacements for each of the nineteen ETS events to create distributed fault slip models. We utilize a non-negative least-squares inversion, so that slip on each fault patch can only have components of reverse and right lateral slip. Surface displacements at GNSS stations are approximated using an elastic half-space dislocation model (Okada, 1992) with a shear modulus of 40 MPa. Each inversion is regularized by applying a smoothing parameter that minimizes the roughness of the slip distribution and data misfit, as determined by the L-curve. Roughness is determined

by the Laplacian of the fault slip model, and the data misfit is defined by the chi-square statistic:

$$\chi^2 = \frac{1}{n_{obs}} \sum_{i=1}^{n_{obs}} \frac{(d_{obs}(i) - d_{pred}(i))^2}{\sigma(i)^2} \quad (1)$$

where n_{obs} is the number of observations, d_{obs} and d_{pred} are the observed and predicted surface displacements, respectively, and σ is the uncertainty of the observations. We estimate the uncertainty for each observation by averaging the standard deviations for the seven days before the transient start date(s) and the seven days after the transient end date(s). We force fault slip to be zero along the perimeter of the fault model. However, since we are exploring ETS at the southern edge of the subduction zone, we do not damp slip on fault patches at the downdip and lateral edges of the fault south of 40.6° N latitude.

We use a megathrust fault model based on the plate contours from McCrory et al. (2012) and determine the updip and downdip limit of our fault model by performing a series of sensitivity tests (Figure S2). We perform these tests with Event 1, since surface displacements during this event span all of southern Cascadia (<43° N latitude). For these tests, we fix the downdip limit of the fault model to 80 km depth and perform the inversion with fault geometries that have progressively shallower updip depth limits. We run a similar set of tests where we fix the updip depth limit of the fault model at the trench (5km depth) and perform the inversion with progressively deeper downdip depths limits. We calculate the data misfit for each inversion according to the chi-square statistic above (Equation 1). The results of our sensitivity tests show that surface displacements in southern Cascadia are not sensitive to slip on the plate interface above 15 km depth or below 55 km depth. However, a comparison of tremor locations and plate depth contours shows that tremor in southernmost Cascadia extends to 75 km depth (Figure 1). If we assume that tremor locations serve as a proxy for slip on the plate interface, then tremor in this region indicates that slip extends past 55 km depth. Therefore, we consider
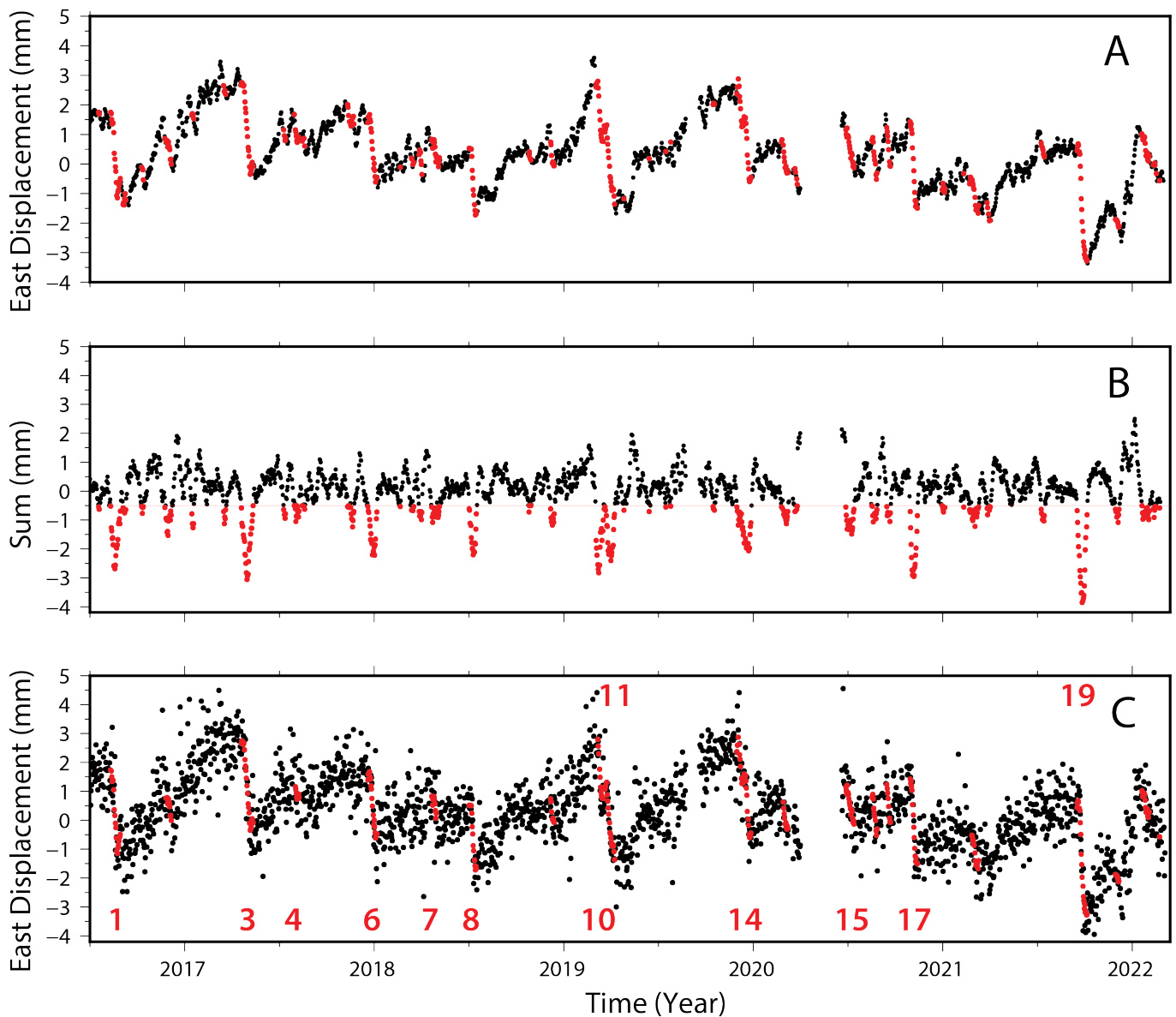
Figure 3   Time series plots for station P343 showing the results of the algorithm used to estimate the timing of ETS transients. **A** Fully processed and smoothed east component time series data (black dots) showing all of the initial days flagged by the algorithm (red dots) that represent potential transient events. **B** Results from the centered 14-day moving sum of the daily displacements (black dots) with all days surpassing the 0.5 mm westward threshold (dashed red line) shown in red. **C** Processed east component time series data without smoothing (black dots) with all of the transients from panel A and B with durations longer than a week shown in red. Displacements associated with ETS events in this study are labeled with red numbers and correlate with the event numbers from Figure 2.

both our sensitivity results and tremor observations to establish a downdip limit of 65 km for our fault model.

It is important to note that other slab models exist for the Cascadia margin. In particular, Slab2 provides three-dimensional fault models for all seismically active global subduction zones (Hayes, 2018). For this work, we choose to use the slab geometry from Mc-Crory et al. (2012) since it focuses solely on Cascadia and explicitly attempts to constrain the complicated fault structure in the MTJ region. Nevertheless, we also perform inversions for several ETS events using the Slab2 model to test how different slab geometries impact the distribution and magnitude of slip along the megathrust. In general, the Slab2 model has less curvature and deeper slab depths in southern Cascadia. For this

second set of inversions, we use the same updip and downdip depth limits of 15 km and 65 km, respectively, for the Slab2 model.

4   Results

We calculate distributed slip models for nineteen ETS events in southern Cascadia (south of 46° N latitude) from mid 2016 to 2022. These events range in moment magnitude from Mw 6.3 to 6.9 (Table S24). Figure 5 shows our slip model for ETS Event 15 (June 2020), which constitutes one of the southernmost events and has an equivalent moment magnitude of Mw 6.5. This slip model indicates that large amounts of slip are not required along the southern edge of the slab to recreate
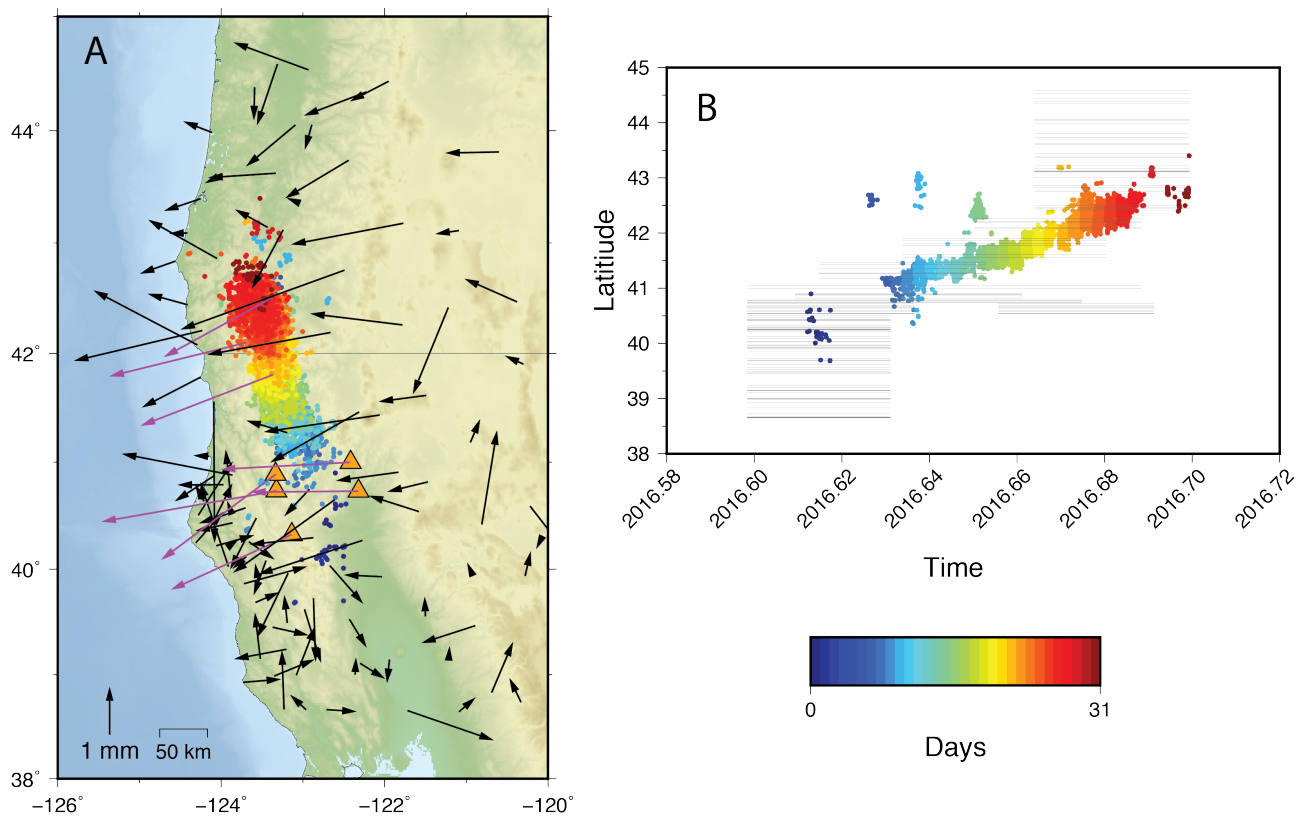
Figure 4 GNSS surface displacements and transient times for ETS Event 1 (August 2016) indicated in Figure 2. **A** Map showing tremor locations (colored dots) and GNSS surface displacements (black vectors) for ETS Event 1. Purple vectors show displacements at index stations and orange triangles indicate the locations of manually added index stations. Tremor is colored according to the number of days since the first tremor occurrence, with the scale provided in the bottom right-hand corner. This event exhibits diminished tremor activity to the south despite a clear signal at the GNSS stations. This diminished tremor activity is likely the result of missed tremor detections stemming from a different tremor detection algorithm and station configuration in southern Cascadia prior to 2017. **B** Plot showing the time periods (horizontal black lines) used to calculate the surface displacements for each GNSS station in panel A by station latitude. Tremor for Event 1 is shown with colored dots and uses the same scale as panel A.

the observed surface displacements. Instead, the maximum slip contour for 22 mm is located >50 km north of the slab edge. It is important to note that the damping of the fault patches at the perimeter of the fault model is not responsible for this lack of slip at the slab edge, as we purposefully do not apply any slip minimization along the southern edges of the fault model (Section 3.2). Slip models for the other eighteen events can be found in the Supplementary Information.

The distributed slip model for ETS Event 15 using the Slab2 fault geometry from Hayes (2018) shows similar results in terms of the fit to the GNSS data and the spatial distribution of slip (Figure S22). Specifically, maximum slip is still concentrated >50 km north of the slab edge. However, the slip magnitudes are lower with the Slab2 model, with the maximum slip magnitude decreasing by 2.3 mm, or 11%, and average slip decreasing by 0.5 mm, or 18%. We also observe consistent results for ETS events located further north for the two plate models, such as for ETS Event 1, with a comparable fit to the GNSS data and consistent spatial distributions (Figure S23). However, the different geometry of the Slab2 model results in slip being up to 10 km deeper along the megathrust in certain locations along strike.

Overall, our results for individual ETS events in south-

ern Cascadia are consistent with the distributed slip models from previous works. In particular, Schmalzle et al. (2014) estimates a similar moment magnitude range of Mw 6.4 to 7.0 for nine ETS events in southern Cascadia. These nine slip models also show comparable slip amplitudes on the megathrust, with the majority of events having maximum slip values of ~20 mm. McKenzie et al. (2020) analyzes three additional ETS events in southern Cascadia and also finds similar slip amplitudes.

To investigate the total slip due to large transient events, we sum the slip distributions for all nineteen ETS events and observe a maximum of 149 mm of total fault slip on the plate interface centered around 40.5° N latitude between 30 to 50 km depth (Figure 6A). Many of the individual ETS events show relatively high slip amplitudes near 40.5° N latitude (Figure S25), suggesting that this region of high slip is a persistent feature and is not the result of a few outlier events. This patch of high slip is located downdip of the shallowly dipping portion of the slab along the northern portion of the slab bend. Furthermore, ETS does not follow the depth contours to the south and thus wrap around the southern portion of the slab bend, nor does it continue towards the southern edge of the slab. Rather, ETS appears to migrate
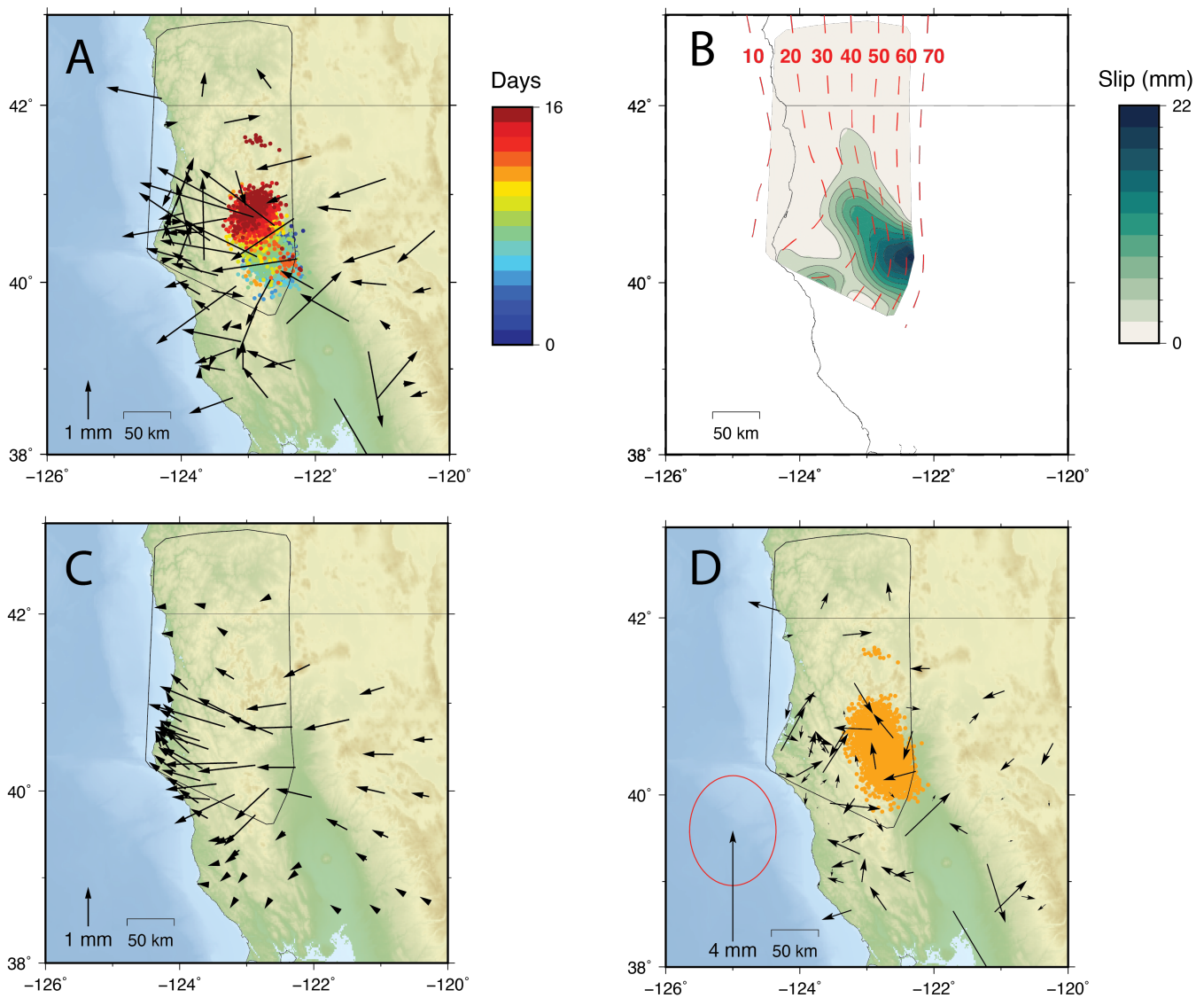
Figure 5 Model results for ETS Event 15 (June 2020) using the plate interface model of McCrory et al. (2012). **A** Vector map showing horizontal surface displacements for ETS event 15. Circles show the location of tremor during the event and are colored by the number of days that passed since the first instance of tremor (June 23, 2020). Black polygon outlines the spatial extent of the slab model. **B** Distributed slip model from our inversion with the contours (black lines with green shading) outlining every 2 mm of fault slip and dashed red lines showing slab depth contours from McCrory et al. (2012). **C** Vector map showing the predicted surface displacements resulting from the slip model in panel B with the black polygon outlining the spatial extent of the slab model. **D** Vector map showing the misfit between the observed and predicted surface displacements and tremor locations with orange circles. Red ellipse shows average 1σ error for all stations, with the average east and north error being 1.6 and 2.0 mm, respectively. Black polygon outlines the spatial extent of the slab model.

downdip, cutting across depth contours on the plate interface and terminating at ~40° N latitude.

For each ETS event that we identified in the PNSN tremor catalog (Figure 2), we found corresponding surface displacements at GNSS stations that are consistent with slow slip on the megathrust. Therefore, slow slip and tremor appear to be coincident in space and time for each of the large ETS events that we studied, within the resolution of the tremor and slip detection. To evaluate the spatial correlation of tremor and slow slip, we segregate the tremor counts by ETS and inter-ETS time periods. The locations of tremor during the nineteen largest ETS events align with the depths of high cumulative fault slip, with the majority of event tremor occurring between 40° and 43° N latitude at 30-55 km depth

(Figure 6B). Tremor that occurs outside of the largest ETS events is located at similar latitudes but is concentrated in a narrower and deeper depth range (Figure 6C). In particular, inter-ETS tremor south of 42° N latitude occurs between 40 and 60 km depth. Similar to slip on the plate interface, neither ETS nor inter-ETS tremor extends to the southern edge of the Gorda slab.

5 Discussion

Our results suggest that ETS behavior is not uniform along strike in southern Cascadia. Rather, we find a concentration of high slip amplitudes between 40° and 41° N latitude and an absence of ETS near the southernmost edge of the subduction zone. In the following sections,
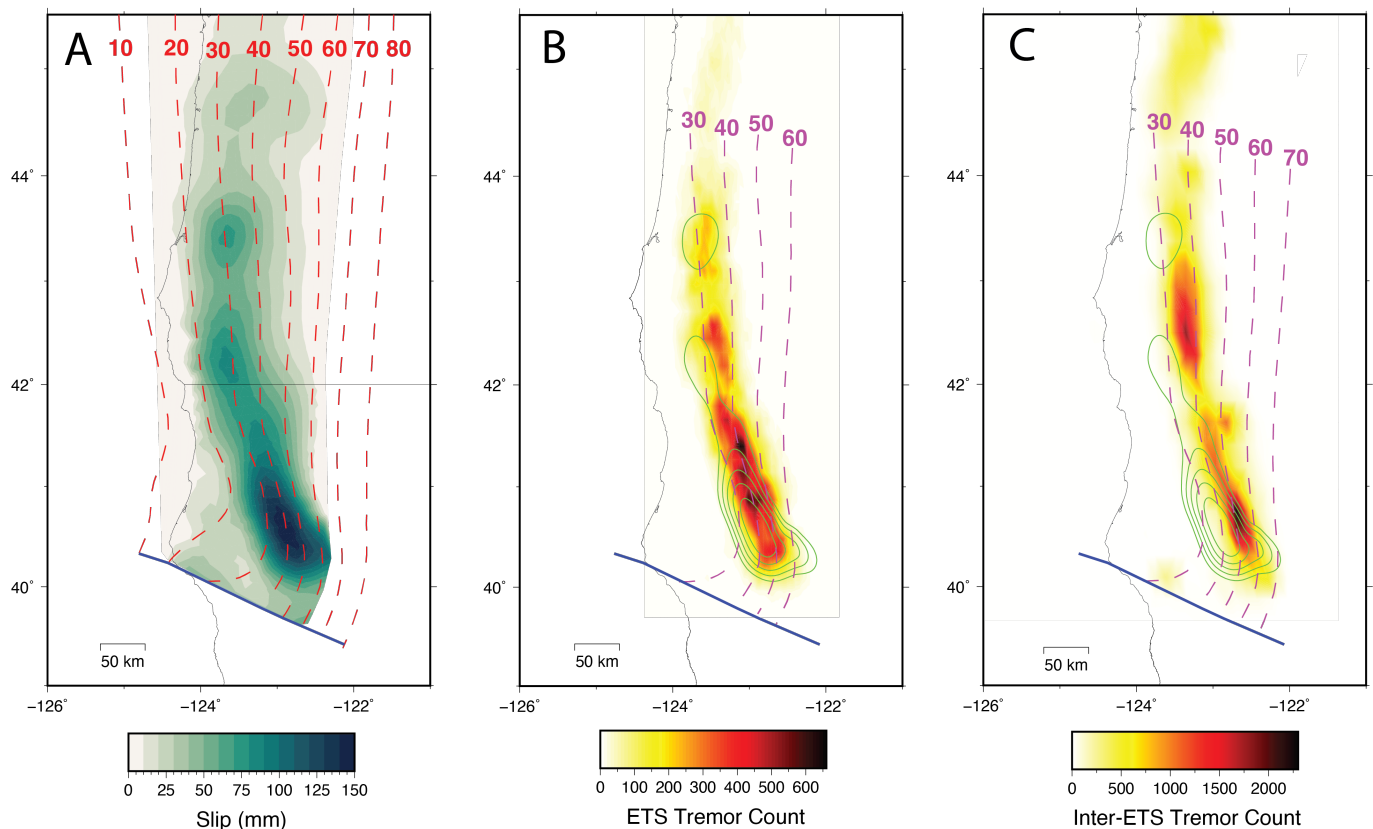
Figure 6 Maps of cumulative slip and tremor results for all of the nineteen ETS events in southern Cascadia. **A** Colored contours show the total fault slip magnitudes on the plate interface from summing all nineteen slip models and dashed red lines and blue line delineate plate depth contours and the southern edge of the Gorda slab from McCrory et al. (2012), respectively. **B** Background colors show the distribution of tremor during the nineteen ETS events, overlain green contours outline total ETS fault slip above 75 mm from panel A with 15 mm intervals, dashed purple lines and blue line delineate plate depth contours and the southern edge of the Gorda slab from McCrory et al. (2012), respectively. **C** Background colors show the distribution of inter-ETS tremor from time periods outside of the nineteen ETS events, overlain green contours outline total slip above 75 mm from panel A with 15 mm intervals, and dashed purple and blue lines delineate plate depth contours and the southern edge of the Gorda slab from McCrory et al. (2012), respectively.

we address how these results compare to previous observations of ETS and different estimates of the location of the slab edge in southern Cascadia (Section 5.1). Additionally, we explore possible explanations for why ETS behavior changes from north to south in southern Cascadia (Sections 5.2 and 5.3) and consider the implications of these changes for the Cascadia subduction zone (Section 5.4).

5.1 Fault Slip Distributions & Previous Observations

5.1.1 ETS and LFEs

Our results show that the cumulative fault slip of nineteen slow slip events along the megathrust reaches a maximum of 149 mm near 40.5° N latitude (Figure 6A). This suggests that large ETS events accommodate up to 85% of the plate convergence in southern Cascadia within the ETS zone, assuming a convergence rate of 32 mm/yr (McCaffrey et al., 2007). Bartlow (2020) uses tremor to identify the timing of ETS in Cascadia and estimates the time-averaged ETS slip rate on the megathrust fault. Results from this work also show relatively high slip rates between 40° and 41° N latitude, confirming

that the majority of strain release in this region between 30 and 50 km depth is accommodated by ETS. However, our results indicate that at least 15% of the plate convergence is accounted for by smaller ETS events (periods of tremor marked by blue dots in Figure 2) and/or by steady aseismic slip. In contrast, Bartlow (2020) estimates that the entire slip budget in this region is facilitated by ETS events, and thus suggests that steady aseismic slip is not needed.

The depth of maximum fault slip and tremor increases from north to south in southern Cascadia as a function of latitude, with relatively high cumulative slip values (>100 mm) occurring at 35 km depth at ~41.5° N latitude and continuing to 60 km depth at ~40.25° N latitude for the McCrory et al. (2012) slab model. This suggests that ETS gradually transitions to deeper depths in southern Cascadia, or that our fault model overestimates the depth to the slab in this region. Delph et al. (2021) offer an alternate estimate of slab depths for southern Cascadia, wherein the McCrory et al. (2012) model is adjusted to fit the location of LFEs. In this model, the slab bend is accentuated south of 42° N latitude at depths ≥40 km, leading to an overall shallower slab model in this region. Therefore, if we use the
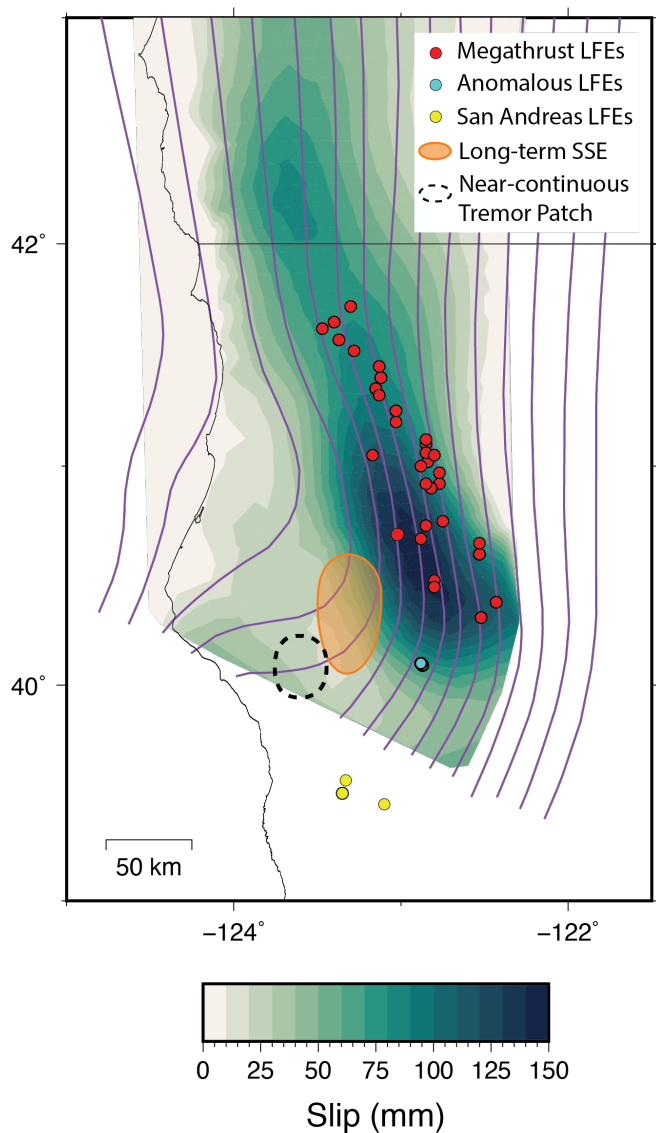
Figure 7 Map of southern Cascadia, with colored contours showing the cumulative fault slip magnitudes from the nineteen ETS events in this study. Yellow and red circles show the location of LFE families associated with the San Andreas fault system and megathrust, respectively (Plourde et al., 2015; Ducellier and Creager, 2022). Overlapping cyan circles show two anomalous LFE families with short recurrence intervals. Orange polygon delineates the 10 mm slip contour for long-term slow slip from Nuyen and Schmidt (2021). Black dashed circle outlines the region of near-continuous tremor from Wech (2021). Purple lines delineate slab depth contours from McCrory et al. (2012) every 5 km starting at 15 km depth.

Delph et al. (2021) slab depths, then high cumulative slip values (>100 mm) do not migrate past 50 km depth at ~40.25° N and the apparent deepening of ETS is less pronounced. Near 40.5° N latitude, maximum cumulative fault slip from ETS events is located just downdip of previously observed long-term slow slip (Figure 7; Nuyen and Schmidt, 2021). This spatial relationship is consistent with events at the Nankai subduction zone in southwest Japan, where ETS is consistently seen downdip of long-term SSEs (e.g. Ozawa, 2017). Farther to the south near ~40° N latitude, ETS fault slip and tremor termi-

nate and do not extend to the southern edge of the Gorda slab. LFEs associated with slow slip along the megathrust exhibit a similar pattern and are not observed south of 40° N latitude (Figure 7; Plourde et al., 2015; Ducellier and Creager, 2022). Together, these observations suggest that the conditions along the plate interface prohibit the occurrence of both LFEs and ETS along the southernmost edge in Cascadia.

5.1.2 Slab Edge Location

While our models suggest that ETS does not extend to the southernmost edge of the Gorda slab, these results are dependent on the McCrory et al. (2012) fault geometry used in the inversions. As a result, other slab geometries could provide different results that show slip associated with ETS events extending farther south. We tested this possibility by calculating distributed slip models for several ETS events using the Slab2 geometry from Hayes (2018), which has a deeper and more planar slab surface in southern Cascadia than the McCrory et al. (2012) model. Ultimately, the models using the Slab2 geometry also show little to no slip on the southernmost edge of the Gorda slab and agree with our initial results. Therefore, the consistency between the results from these two different slab models supports the idea that ETS does not occur in southernmost Cascadia.

The distance between the southern extent of ETS and the edge of the Cascadia subduction zone is dependent on the location of the southern edge of the Gorda slab. In this work, we reference the slab edge from McCrory et al. (2004), which is based on the pattern of first-motion readings at seismic stations in northern California. A similar slab edge location is also inferred by Jachens and Griscom (1983) from gravity data. The agreement between these two independent studies, which employ distinct datasets and methods, gives us some confidence in the location of the slab edge. However, several other studies have focused on locating the slab edge beneath Northern California and the results from these works reveal a range of interpretations with slab edges farther to the north (Figure 8; Beaudoin et al., 1998; Furlong and Schwartz, 2004; Liu et al., 2012; Verdonck and Zandt, 1994).

The discrepancy between slab edge estimates in southern Cascadia likely stems from the various methods that are used to image the underlying structure, which cover a range of spatial scales and resolutions. For example, reflection and refraction studies are good for distinguishing sharp boundaries within the lithosphere (e.g. Beaudoin et al., 1998), whereas tomographic models excel at recognizing larger-scale spatial variations in seismic velocity (e.g. Liu et al., 2012). The dimensionality of these methods also varies between 1-dimensional profiles (e.g. receiver functions, dispersion curves), 2-dimensional cross-sections (e.g. reflection, refraction), and 3-dimensional models (e.g. tomography). Additionally, studies that utilize earthquake hypocenters to determine the lithospheric structure in the region are highly dependent on *a priori* velocity models, which can vary between studies. Lastly, several studies utilize gravity data (e.g. Jachens and Griscom,
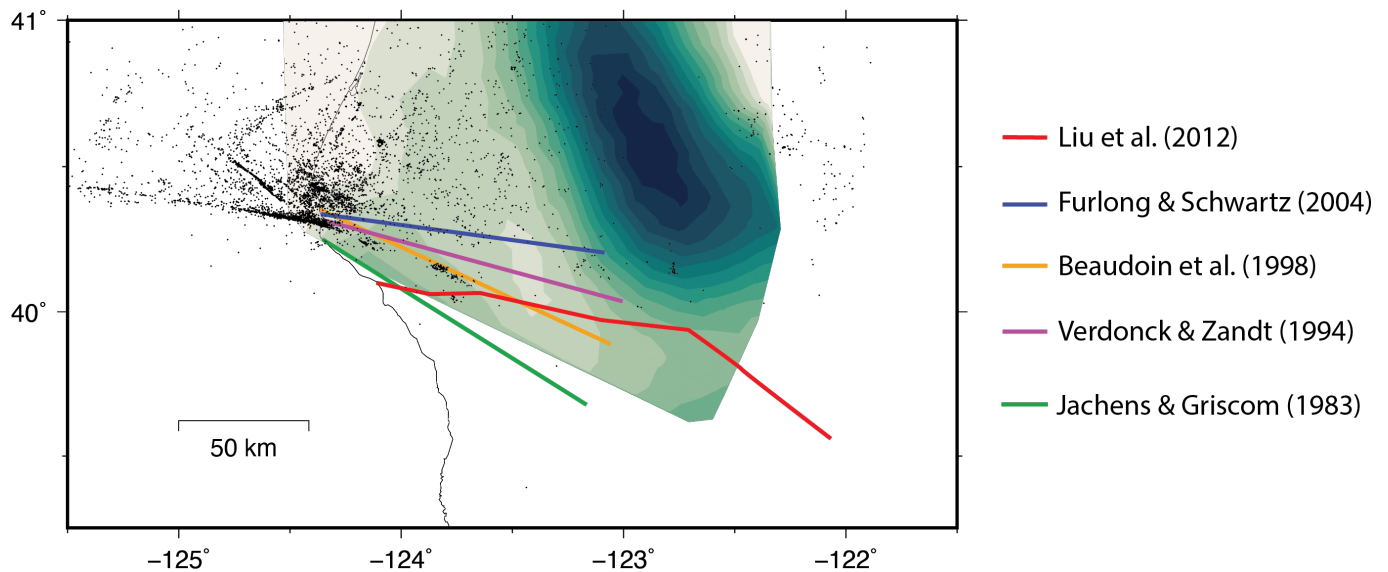
Figure 8 Map of southern Cascadia with colored lines delineating the estimated location of the slab edge from the five studies listed next to the panel. Colored contours show the cumulative fault slip magnitudes from the nineteen ETS events in this study and black dots show the earthquake locations from Guo et al. (2021).

1983; Beaudoin et al., 1998), which is most sensitive to density contrasts in the subsurface. As a result, seismic and gravity data may resolve different boundaries within the lithosphere and lead to different structural interpretations. However, subsurface structural models constrained by gravity data are non-unique and add further uncertainty to the position of the slab edge. This is exemplified by the gravity models presented in Beaudoin et al. (1998), which suggests an uncertainty of ±25 km in the position of the slab edge. Together, these differences in the resolution and scope of different methods likely account for some of the variation in the slab edge estimates. Nevertheless, the majority of these estimates place the slab edge at least 50 km south of the maximum slip contour and further confirm that ETS does not occur at the edge of the subduction zone (Figure 8).

5.2 Geometric Controls on ETS

As discussed in Section 2.1, southernmost Cascadia exhibits an irregular megathrust structure that is associated with a bend in the Gorda slab. We propose that this complex geometry impacts ETS behavior in southern Cascadia, leading to a concentration of high slip amplitudes between 40° and 41° N latitude and an absence of ETS near the southernmost edge of the subduction zone. Ultimately, we believe that the non-planar geometry of the Gordo slab could affect ETS in this region by impacting 1) the orientation of the fault relative to convergence, 2) the width of the ETS zone, 3) shear-strength heterogeneity along the megathrust fault, and 4) fluid migration patterns along the plate interface.

5.2.1 Fault Orientation & Width of ETS Zone

In northern Cascadia, the Juan de Fuca slab exhibits an along-strike bend beneath northern Washington and

southern British Columbia that is comparable to the bend in the Gorda slab. Observations of ETS events in northern Cascadia indicate that the axis of this bend, located in northwestern Washington, exhibits higher amounts of ETS fault slip per event than the portions of the slab located directly to the north or south (Schmidt and Gao, 2010). A similar trend is also observed at the Nankai subduction zone, where higher cumulative slip rates are found near slab bends beneath Shikoku and Ise Bay (Nishimura et al., 2013; Kano and Kato, 2020). Our results also fit into this pattern, as we observe a patch of high cumulative fault slip along the northern limb of the bend in the Gorda slab between 40° and 41° N latitude. Together, these observations suggest that the slab bend in the Gorda plate may influence the distribution of slip amplitude in southern Cascadia.

The mechanisms that promote higher slip amplitudes per event near the slab bend may relate to the optimal orientation of the plate interface relative to convergence. Li and Liu (2016) present rate-and-state-based numerical models of SSEs in northern Cascadia that are able to recreate higher moment rates and cumulative slip amounts in the central portion of the slab bend. These simulations support previous work that suggests slip amplitude is proportional to the model parameter W/h^*, where W is the along-dip distance of the velocity-weakening ETS zone and h^* is the minimum size for unstable slip, or characteristic nucleation size (Liu and Rice, 2009). If we assume that the ETS zone is bounded by specific depth contours, then this relationship would imply that a steeper dipping slab would have smaller ETS slip amplitudes due to a narrower ETS zone compared to a shallower dipping slab with a wider ETS zone. However, this finding does not appear to explain the concentration of high slip amplitudes along the northern limb of the slab bend in southern Cascadia, since this predicted patch of high slip is located on a rela-

tively steeply dipping portion of the slab according to the McCrory et al. (2012) model (Figure 7). Nevertheless, Li and Liu (2016) present an alternative model, where the width of the ETS zone is held constant. These model results show that while slip amplitudes are still inversely proportional to fault dip, they are also highest on fault patches that strike perpendicular to the convergence direction. Therefore, higher slip rates near the northern bend in the Gorda slab from our distributed slip models may indicate that this portion of the fault is more optimally oriented relative to convergence. Given that the northern bend in the Gorda slab strikes broadly northwest, this hypothesis aligns with the current understanding of convergence dynamics in southern Cascadia, which infers oblique northeast subduction of the Gorda slab relative to the North American plate (McKenzie and Furlong, 2021).

Our results show that high ETS fault slip amplitudes do not extend around the southern portion of the slab bend in southernmost Cascadia (Figure 9), and we propose that a narrowing of the ETS zone due to warping of the slab edge may provide an explanation for this observation. Several studies propose that the edge of the Gorda slab dips to the south-southeast (suborthogonal to subduction direction) with dip angles of up to 12° (Furlong and Schwartz, 2004; Verdonck and Zandt, 1994). This southward dip, together with the slab bend, may lead to a steeper plate interface near the slab edge. As noted above, if we assume that ETS falls within a specific depth range along the plate interface, then a steeper slab dip would lead to a narrower ETS zone near the southern edge of the slab. Following the ETS models of Liu and Rice (2007, 2009), a narrower ETS zone would lower the W/h^* parameter and lead to smaller slow slip amplitudes in southernmost Cascadia. Additionally, models from Liu and Rice (2007, 2009) find that relatively small values of W/h^* (<2.16) lead to decaying oscillatory responses along the fault, which do not result in slow slip events. Therefore, low fault slip rates in southernmost Cascadia may be due to a narrow ETS zone that is incapable of producing large ETS events.

5.2.2 Shear Strength Heterogeneity on a Curved Fault

A complex geometry near the slab edge may also influence how far slow slip can propagate across the fault and help to explain the lack of ETS we observe in southernmost Cascadia. Global comparisons of subduction zone systems show that the along-dip curvature of megathrust faults generally scales with maximum earthquake magnitude (Bletery et al., 2016; Plescia and Hayes, 2020). Bletery et al. (2016, 2017) attribute this relationship to the shear-strength heterogeneity across a fault, proposing that shear-strength heterogeneity increases as a function of fault curvature and thus limits the magnitude of megathrust earthquakes by acting as a natural barrier for earthquake slip propagation. Specifically, slip propagation may be halted by localized regions of relatively high shear strength associated with stress heterogeneity (Wang and Bilek, 2014). If we assume that this theory also applies to slow slip
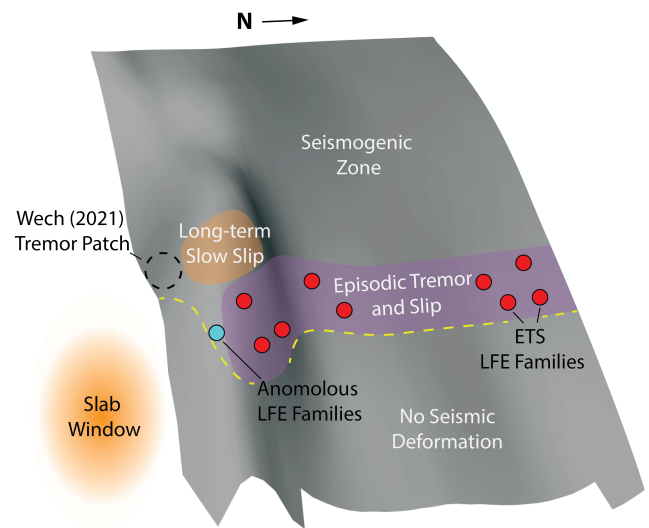
Figure 9 Schematic illustrating the distribution of deformational regimes and observed phenomena along the three-dimensional plate interface in southern Cascadia. The perspective is looking towards the northwest onto the warped geometry of the Gorda slab (gray surface). The dashed yellow line indicates the maximum depth at which seismic deformation can occur along the plate interface. We propose that the heating of the slab edge by an inferred slab window (orange halo to the south of the slab edge) results in the shallowing of the seismic-aseismic transition, inhibiting seismic deformation and ETS near the southernmost edge of the slab. Other symbols are the same as Figure 7. Slab geometry is based on McCrory et al. (2012) and includes vertical exaggeration.

propagation, then our results suggest that an increasingly curved slab geometry in southernmost Cascadia may produce high shear-strength heterogeneity near the slab edge, which limits the propagation and size of ETS events in this region.

5.2.3 Fluid Migration Pathways on a Curved Fault

The curved geometry of the Gorda slab may also impact the migration of fluids along the plate interface and help generate the high slip amplitudes we observe between 40° and 41° N latitude. Geophysical evidence for a low-velocity zone (LVZ) along numerous megathrust faults suggests that high pore-fluid pressures exist along the plate interface at ETS depths (e.g. Audet et al., 2009). As a result, high pore-fluid pressures are often invoked as a prerequisite for possible ETS mechanisms, such as dilatant strengthening (e.g. Segall et al., 2010). Morishige and van Keken (2017) present 3-D numerical models of fluid migration along curved slab geometries and find that fluid paths concentrate in regions where the slab has a convex shape along-strike, leading to increased porosity values near slab bends. Therefore, the relatively high slip amplitudes that we observe around the northern bend in the Gorda slab may also be explained by the focusing of fluids in this region. However, it is still unclear if and how fault slip amplitudes scale with the magnitude of pore pressure along the plate interface.

5.3 Temperature Controls on ETS

As discussed in Section 2.2, thermal models for southern Cascadia suggest that the presence of a slab window south of the MTJ leads to higher temperatures in the continental lithosphere and descending Gorda slab (Goes et al., 1997; Guzofski and Furlong, 2002; Popov et al., 2012; van Wijk, 2001). Therefore, we suggest that elevated temperatures along the megathrust due to heat transfer from the slab window inhibit the occurrence of ETS in southernmost Cascadia. Specifically, we propose that higher temperatures could lead to a shallower seismic-aseismic transition in southern Cascadia and alter the location of fluid release from the subducting slab.

5.3.1 Seismic-Aseismic Transition Near the Slab Window

Deformation along the plate interface is accommodated by a continuum of seismic and aseismic slip modes along the megathrust (Peng and Gomberg, 2010). In general, ETS occurs in the seismic-aseismic transition zone that is located updip of the aseismic creeping portion of the fault and downdip of the seismogenic locked zone (Schwartz and Rokosky, 2007). At warm subduction zones, such as Cascadia, the depth of this seismic-aseismic transition is thought to be largely controlled by temperature (e.g. Hyndman and Wang, 1993; Oleskevich et al., 1999). Therefore, changes in a subduction zone's thermal gradient may impact the depth distribution of different deformational regimes along the plate interface. Specifically, higher temperatures in southernmost Cascadia due to heating from the adjacent slab window may shift the seismic-aseismic transition updip along the megathrust (Figure 9). Therefore, our results, which show little to no ETS activity in southernmost Cascadia, could mean that deformation within the typical ETS zone (i.e. along the plate interface at 35-60 km depth) may be dominated by solely aseismic slip and not ETS due to a relatively shallow seismic-aseismic boundary. This shift in deformational regimes may also explain why LFEs along the megathrust are not observed south of 40° N latitude (Figure 7), since these events are associated with seismic shear slip (Ide et al., 2007; Plourde et al., 2015; Shelly et al., 2007). Furthermore, the relatively short recurrence intervals for the southernmost megathrust LFE family may reflect north-to-south (along-strike) weakening of the plate interface due to increasing temperatures along the megathrust (Ducellier and Creager, 2022).

Following this reasoning, we might expect to observe ETS at shallower depths (<30 km) in southernmost Cascadia near the slab edge, where temperatures are low enough along the megathrust to potentially facilitate seismic deformation in the form of tremor. Although shallower ETS events are not observed, Wech (2021) identifies a temporally near-continuous patch of tremor in this region with an unknown source (Figure 9). If this tremor does originate from the plate interface, then it may indicate the presence of ETS at ~30 km depth and support the notion that ETS is transferred updip due to a higher thermal gradient in southern Cascadia that

warms the slab edge. Furthermore, the near continuous activity of this tremor patch suggests that it would represent the downdip limit of the ETS zone, where the fault cannot accumulate large amounts of stress and fails via small, frequent slip events (Wech and Creager, 2011).

5.3.2 Fluid Release Related to Elevated Temperatures

As described in Section 5.2.3, high pore-fluid pressures are thought to exist along portions of the plate interface at subduction zones and play a critical role in the mechanisms for ETS (e.g. Audet and Kim, 2016). Fluids at the plate interface are sourced from the crust and mantle of the subducting slab, which release mineral-bound water through a variety of dehydration reactions (Peacock, 1993; Rüpke et al., 2004). However, the depth at which these reactions occur is dependent on the pressure-temperature (P-T) path of the slab, which can vary substantially between subduction zones (Peacock, 2009). Thermodynamic models for southern Cascadia at ~42° N latitude indicate that average mid-ocean ridge basalts (MORB) dehydrate 1-1.5 wt% H_2O at ~35 km depth and suggest that in-situ fluid release is the dominant water source for ETS in this region (Condit et al., 2020). These models also show that higher slab temperatures lead to the slab releasing fluids at shallower depths. For example, increasing the temperature path of the slab by 50 °C results in fluids being released at ~5 km shallower depths (Condit et al., 2020). Therefore, heating of the Gorda slab from the adjacent slab window may result in fluids being released at shallower depths along the megathrust in southernmost Cascadia. Depending on the thermal gradient of the slab, fluids may be released updip of typical ETS depths, limiting high pore-fluid pressures from developing along the plate interface in the expected ETS zone. As a result, the lack of ETS activity that we observe in southernmost Cascadia could signal that ETS is being inhibited by low pore-fluid pressures along the plate interface caused by insufficient in-situ fluid release from the warm Gorda slab at typical ETS depths.

Fluid release is not a single event and can occur gradually and at various temperatures and depths along the plate interface (van van Keken et al., 2011). Therefore, increases in slab temperature do not preclude the possibility of fluids migrating into the ETS zone from other portions of the subduction zone. In particular, fluids released deeper on the plate interface from dehydration reactions that take place at higher P-T conditions could travel updip to ETS depths (Katayama et al., 2012; Hyndman et al., 2015). Additional fluids may also be sourced from the serpentinized mantle wedge. Specifically, Kirby et al. (2014) shows that heating of the relict mantle wedge in the slab window can lead to the release of water through the dehydration of serpentine. This dehydration may also occur in the current subduction zone mantle wedge if temperatures have increased to the point of making serpentine thermally unstable. However, it is unclear whether fluids released from the relict or current mantle wedge could supply fluids to the plate interface or would migrate upwards into the

overlying crust. Nevertheless, high pore-fluid pressures generated by the updip migration of fluids may not be enough to facilitate ETS if the appropriate fault rheology is not present. For example, heating from the slab window may promote ductile deformation that prohibits shear faulting and tremor along the plate interface even if high pore-fluid pressures are present (Shelly et al., 2007).

5.4   Synthesis and Implications

An analysis of nineteen ETS events suggests that fault slip associated with ETS does not extend to the southern edge of the Gorda slab. Therefore, we hypothesize that the southern termination of ETS marks a major shift in megathrust properties that is tied to changes in the geometry of the Gorda slab and/or thermal conditions near the edge of the subduction zone (Figure 9). In terms of slab geometry, a proposed southward dip at the southern edge of the Gorda slab may combine with the slab bend, resulting in a three-dimensional curling of the slab (Furlong and Schwartz, 2004; Verdonck and Zandt, 1994). This complex geometry could lead to 1) a narrower ETS zone that does not host large amounts of slip (Liu and Rice, 2007, 2009) or 2) heterogeneous shear-strength across the fault that acts as a barrier for ETS propagation (Bletery et al., 2016, 2017). In terms of subduction zone temperatures, numerous models suggest that the slab window south of the MTJ actively transfers heat to the adjacent Gorda slab and North American lithosphere (Goes et al., 1997; Guzofski and Furlong, 2002; Popov et al., 2012; van Wijk, 2001). Increases in subduction zone temperatures in Cascadia may 1) shift the depth of the seismic-aseismic transition updip (Groom & Thorkelson, 2007) or 2) cause the Gorda slab to release fluids at shallower depths above the ETS zone (Condit et al., 2020). Overall, these proposed changes in subduction zone properties suggest that solely aseismic deformation takes place along the plate interface below 35 km depth in southernmost Cascadia (south of 40° N latitude).

It is important to note that the processes presented above are likely interconnected. For example, the three-dimensional geometry of the slab edge should influence how slab temperatures evolve in response to the slab window, which in turn impacts the location of different deformational modes along the plate interface. Therefore, better constraints on the individual components of the subduction zone system, e.g. the geometry of the slab edge, and future modeling of the interactions between the subduction zone and slab window are necessary to determine the relative importance of each process. Outstanding questions that future models could address include 1) how are slab temperatures impacted by different slab edge geometries, 2) what is the spatiotemporal scale of subduction zone heating and how is it influenced by different mantle flow patterns in the slab window (e.g. upwelling vs. toroidal flow), and 3) what is the P-T path for the non-uniform portion of the Gorda slab and what does that mean for the depth of fluid release? Furthermore, additional work on the near-continuous tremor patch found by Wech (2021)

would also help illuminate the state of ETS in southernmost Cascadia. For example, a moment tensor analysis of individual LFEs could help to determine the source fault of the tremor and clarify if ETS is shifted updip near the edge of the Gorda slab.

The results from this work are relevant to other systems that have a complex slab geometry and/or slab window near the lateral edge of a subducting plate. For instance, the northern terminus of the Cascadia subduction zone is defined by the lateral edge of the Explorer plate beneath northern Vancouver Island. The distribution of earthquake hypocenters in this region reveals significant warping of the subducted Explorer slab, wherein the plate interface deepens ~15 km along strike over a distance of <100 km (Hutchinson et al., 2020). Geochemical analysis of basalts from the northern Cascade Arc also suggests that a slab gap or tear exists between the Juan de Fuca and Explorer plates, allowing for enriched asthenosphere to flow into the Cascadia mantle wedge (Mullen and Weis, 2015). Observations of ETS in northernmost Cascadia show a nonuniform distribution of tremor, including decreased tremor activity at the northern end of the subduction zone and a prominent gap in tremor near 49.5° N latitude (Kao et al., 2009). Therefore, ETS behavior in northernmost Cascadia may be influenced by the warped geometry of the Explorer plate, similar to what we observe in southernmost Cascadia and the Gorda plate. In southern Chile, the varying dips and depth extents of the subducting Nazca and Antarctic plates beneath the South American plate help to form a slab window at the Chile triple junction (Russo et al., 2010). In the southernmost portion of the Chilean subduction zone, the depth of tremor along the Nazca plate shallows ~20 km as it approaches the edge of the subduction zone and the slab window (Ide, 2012). This shallowing of tremor may correlate with plate age and temperature (Ide, 2012), or it may represent another locale where increased temperatures from a slab window are impacting the depth of ETS at the lateral edge of a subduction zone.

6   Conclusions

We analyze 5.5 years of tremor and GNSS time series data and identify 19 large ETS events in southern Cascadia from 2016.5-2022. Distributed slip models indicate that fault slip and tremor during these events are spatially correlated, with tremor during the largest ETS events falling slightly updip of inter-ETS tremor. Our models also show that ETS terminates near 40° N latitude and does not extend to the southern edge of the Gorda slab. Therefore, we hypothesize that seismic slip (i.e. tremor) does not take place along the plate interface below 35 km depth in southernmost Cascadia and that the southern boundary of ETS reflects changes in megathrust properties that are linked to changes in slab geometry and/or subduction zone temperatures. Possible factors that influence ETS in southern Cascadia include the depth at which the Gorda slab releases fluids, the width of the ETS zone, the optimal orientation of the plate interface relative to local convergence, the

depth of the seismic-aseismic transition, the migration patterns of fluids within the subduction zone, and the pattern of shear-strength across the megathrust fault. Future modeling studies that explore the geometric and thermal structure of the Gorda slab and southernmost Cascadia subduction zone are needed to discern the primary controls on ETS in this region.

Acknowledgements

7 Data and Code Availability

Distributed slip model results for the nineteen ETS events are available at Mendeley Data, http://dx.doi.org/10.17632/s9d4gbk3bn.1.

8 Competing Interests

The authors have no competing interests.

References

Atwater, T. Implications of Plate Tectonics for the Cenozoic Tectonic Evolution of Western North America. *Geological Society of America Bulletin*, 81(12):3513, 1970. doi: 10.1130/0016-7606(1970)81[3513:ioptft]2.0.co;2.

Audet, P. and Kim, Y. Teleseismic constraints on the geological environment of deep episodic slow earthquakes in subduction zone forearcs: A review. *Tectonophysics*, 670:1–15, Feb. 2016. doi: 10.1016/j.tecto.2016.01.005.

Audet, P., Bostock, M. G., Christensen, N. I., and Peacock, S. M. Seismic evidence for overpressured subducted oceanic crust and megathrust fault sealing. *Nature*, 457(7225):76–78, Jan. 2009. doi: 10.1038/nature07650.

Bartlow, N. M. A Long-Term View of Episodic Tremor and Slip in Cascadia. *Geophysical Research Letters*, 47(3), Feb. 2020. doi: 10.1029/2019gl085303.

Beaudoin, B. C., Hole, J. A., Klemperer, S. L., and Tréhu, A. M. Location of the southern edge of the Gorda slab and evidence for an adjacent asthenospheric window: Results from seismic profiling and gravity. *Journal of Geophysical Research: Solid Earth*, 103(B12):30101–30115, Dec. 1998. doi: 10.1029/98jb02231.

Benz, H. M., Zandt, G., and Oppenheimer, D. H. Lithospheric structure of northern California from teleseismic images of the upper mantle. *Journal of Geophysical Research: Solid Earth*, 97(B4): 4791–4807, Apr. 1992. doi: 10.1029/92jb00067.

Bletery, Q., Thomas, A. M., Rempel, A. W., Karlstrom, L., Sladen, A., and De Barros, L. Mega-earthquakes rupture flat megathrusts. *Science*, 354(6315):1027–1031, Nov. 2016. doi: 10.1126/science.aag0482.

Bletery, Q., Thomas, A. M., Rempel, A. W., and Hardebeck, J. L. Imaging Shear Strength Along Subduction Faults. *Geophysical Research Letters*, 44(22), Nov. 2017. doi: 10.1002/2017gl075501.

Bodmer, M., Toomey, D. R., Hooft, E. E. E., and Schmandt, B. Buoyant Asthenosphere Beneath Cascadia Influences Megathrust Segmentation. *Geophysical Research Letters*, 45(14):6954–6962, July 2018. doi: 10.1029/2018gl078700.

Boyarko, D. C. and Brudzinski, M. R. Spatial and temporal patterns of nonvolcanic tremor along the southern Cascadia subduction zone. *Journal of Geophysical Research: Solid Earth*, 115 (B8), Aug. 2010. doi: 10.1029/2008jb006064.

Brudzinski, M. R. and Allen, R. M. Segmentation in episodic tremor and slip all along Cascadia. *Geology*, 35(10):907–910, 10 2007. doi: 10.1130/G23740A.1.

Chaytor, J. D., Goldfinger, C., Dziak, R. P., and Fox, C. G. Active deformation of the Gorda plate: Constraining deformation models with new geophysical data. *Geology*, 32(4):353, 2004. doi: 10.1130/g20178.2.

Condit, C. B., Guevara, V. E., Delph, J. R., and French, M. E. Slab dehydration in warm subduction zones at depths of episodic slip and tremor. *Earth and Planetary Science Letters*, 552:116601, Dec. 2020. doi: 10.1016/j.epsl.2020.116601.

Delph, J. R., Thomas, A. M., and Levander, A. Subcretionary tectonics: Linking variability in the expression of subduction along the Cascadia forearc. *Earth and Planetary Science Letters*, 556: 116724, Feb. 2021. doi: 10.1016/j.epsl.2020.116724.

Dickinson, W. R. and Snyder, W. S. Geometry of triple junctions related to San Andreas Transform. *Journal of Geophysical Research: Solid Earth*, 84(B2):561–572, Feb. 1979a. doi: 10.1029/jb084ib02p00561.

Dickinson, W. R. and Snyder, W. S. Geometry of Subducted Slabs Related to San Andreas Transform. *The Journal of Geology*, 87 (6):609–627, Nov. 1979b. doi: 10.1086/628456.

Dong, D., Fang, P., Bock, Y., Webb, F., Prawirodirdjo, L., Kedar, S., and Jamason, P. Spatiotemporal filtering using principal component analysis and Karhunen-Loeve expansion approaches for regional GPS network analysis. *Journal of Geophysical Research: Solid Earth*, 111(B3), Mar. 2006. doi: 10.1029/2005jb003806.

Ducellier, A. and Creager, K. C. An 8-Year-Long Low-Frequency Earthquake Catalog for Southern Cascadia. *Journal of Geophysical Research: Solid Earth*, 127(4), Apr. 2022. doi: 10.1029/2021jb022986.

Furlong, K. P. and Schwartz, S. Y. INFLUENCE OF THE MENDOCINO TRIPLE JUNCTION ON THE TECTONICS OF COASTAL CALIFORNIA. *Annual Review of Earth and Planetary Sciences*, 32(1):403–433, May 2004. doi: 10.1146/annurev.earth.32.101802.120252.

Goes, S., Govers, R., Schwartz, S., and Furlong, K. Three-dimensional thermal modeling for the Mendocino Triple Junction area. *Earth and Planetary Science Letters*, 148(1–2):45–57, Apr. 1997. doi: 10.1016/s0012-821x(97)00044-7.

Gomberg, J. Slow-slip phenomena in Cascadia from 2007 and beyond: A review. *Geological Society of America Bulletin*, 122(7–8): 963–978, Mar. 2010. doi: 10.1130/b30287.1.

Groome, W. G. and Thorkelson, D. J. The three-dimensional thermo-mechanical signature of ridge subduction and slab window migration. *Tectonophysics*, 464(1–4):70–83, Jan. 2009. doi: 10.1016/j.tecto.2008.07.003.

Guo, H., McGuire, J. J., and Zhang, H. Correlation of porosity variations and rheological transitions on the southern Cascadia megathrust. *Nature Geoscience*, 14(5):341–348, May 2021. doi: 10.1038/s41561-021-00740-1.

Guzofski, C. A. and Furlong, K. P. Migration of the Mendocino triple

junction and ephemeral crustal deformation: Implications for California Coast range heat flow. *Geophysical Research Letters*, 29(1), Jan. 2002. doi: 10.1029/2001gl013614.

Hayes, G. Slab2 - A Comprehensive Subduction Zone Geometry Model, 2018. doi: 10.5066/F7PV6JNV.

Herring, T. A., Melbourne, T. I., Murray, M. H., Floyd, M. A., Szeliga, W. M., King, R. W., Phillips, D. A., Puskas, C. M., Santillan, M., and Wang, L. Plate Boundary Observatory and related networks: GPS data analysis methods and geodetic products. *Reviews of Geophysics*, 54(4):759–808, 2016.

Hutchinson, J., Kao, H., Riedel, M., Obana, K., Wang, K., Kodaira, S., Takahashi, T., and Yamamoto, Y. Significant geometric variation of the subducted plate beneath the northernmost Cascadia subduction zone and its tectonic implications as revealed by the 2014 M 6.4 earthquake sequence. *Earth and Planetary Science Letters*, 551:116569, Dec. 2020. doi: 10.1016/j.epsl.2020.116569.

Hyndman, R. D. and Wang, K. Thermal constraints on the zone of major thrust earthquake failure: The Cascadia Subduction Zone. *Journal of Geophysical Research: Solid Earth*, 98(B2): 2039–2060, Feb. 1993. doi: 10.1029/92jb02279.

Hyndman, R. D., McCrory, P. A., Wech, A., Kao, H., and Ague, J. Cascadia subducting plate fluids channelled to fore-arc mantle corner: ETS and silica deposition. *Journal of Geophysical Research: Solid Earth*, 120(6):4344–4358, June 2015. doi: 10.1002/2015jb011920.

Ide, S. Variety and spatial heterogeneity of tectonic tremor worldwide. *Journal of Geophysical Research: Solid Earth*, 117(B3), Mar. 2012. doi: 10.1029/2011jb008840.

Ide, S., Shelly, D. R., and Beroza, G. C. Mechanism of deep low frequency earthquakes: Further evidence that deep nonvolcanic tremor is generated by shear slip on the plate interface. *Geophysical Research Letters*, 34(3), Feb. 2007. doi: 10.1029/2006gl028890.

Ismat, Z., Putera, H., and Patzkowsky, S. Internal deformation of the Gorda plate and its tectonic significance within the Cascadia subduction zone. *Journal of Structural Geology*, 161:104643, Aug. 2022. doi: 10.1016/j.jsg.2022.104643.

Ito, Y., Obara, K., Shiomi, K., Sekine, S., and Hirose, H. Slow Earthquakes Coincident with Episodic Tremors and Slow Slip Events. *Science*, 315(5811):503–506, Jan. 2007. doi: 10.1126/science.1134454.

Jachens, R. C. and Griscom, A. Three-dimensional geometry of the Gorda Plate beneath northern California. *Journal of Geophysical Research: Solid Earth*, 88(B11):9375–9392, Nov. 1983. doi: 10.1029/jb088ib11p09375.

Kano, M. and Kato, A. Detailed Spatial Slip Distribution for Short-Term Slow Slip Events Along the Nankai Subduction Zone, Southwest Japan. *Journal of Geophysical Research: Solid Earth*, 125(7), July 2020. doi: 10.1029/2020jb019613.

Kao, H., Shan, S., Dragert, H., and Rogers, G. Northern Cascadia episodic tremor and slip: A decade of tremor observations from 1997 to 2007. *Journal of Geophysical Research: Solid Earth*, 114 (B11), Nov. 2009. doi: 10.1029/2008jb006046.

Katayama, I., Terada, T., Okazaki, K., and Tanikawa, W. Episodic tremor and slow slip potentially linked to permeability contrasts at the Moho. *Nature Geoscience*, 5(10):731–734, Sept. 2012. doi: 10.1038/ngeo1559.

Kirby, S. H., Wang, K., and Brocher, T. M. A large mantle water source for the northern San Andreas fault system: a ghost of subduction past. *Earth, Planets and Space*, 66(1), July 2014. doi: 10.1186/1880-5981-66-67.

Lachenbruch, A. H. and Sass, J. H. Heat flow and energetics of the San Andreas Fault Zone. *Journal of Geophysical*

Research: Solid Earth, 85(B11):6185–6222, Nov. 1980. doi: 10.1029/jb085ib11p06185.

Li, D. and Liu, Y. Spatiotemporal evolution of slow slip events in a nonplanar fault model for northern Cascadia subduction zone. *Journal of Geophysical Research: Solid Earth*, 121(9):6828–6845, Sept. 2016. doi: 10.1002/2016jb012857.

Liu, K., Levander, A., Zhai, Y., Porritt, R. W., and Allen, R. M. Asthenospheric flow and lithospheric evolution near the Mendocino Triple Junction. *Earth and Planetary Science Letters*, 323–324: 60–71, Mar. 2012. doi: 10.1016/j.epsl.2012.01.020.

Liu, Y. and Rice, J. R. Spontaneous and triggered aseismic deformation transients in a subduction fault model. *Journal of Geophysical Research: Solid Earth*, 112(B9), Sept. 2007. doi: 10.1029/2007jb004930.

Liu, Y. and Rice, J. R. Slow slip predictions based on granite and gabbro friction data compared to GPS measurements in northern Cascadia. *Journal of Geophysical Research: Solid Earth*, 114 (B9), 2009. doi: https://doi.org/10.1029/2008JB006142.

McCaffrey, R., Qamar, A. I., King, R. W., Wells, R., Khazaradze, G., Williams, C. A., Stevens, C. W., Vollick, J. J., and Zwick, P. C. Fault locking, block rotation and crustal deformation in the Pacific Northwest. *Geophysical Journal International*, 169(3): 1315–1340, June 2007. doi: 10.1111/j.1365-246x.2007.03371.x.

McCrory, P. A., Blair, J. L., Oppenheimer, D. H., and Walter, S. R. *Depth to the Juan de Fuca slab beneath the Cascadia subduction margin– A 3-D model for sorting earthquakes*. 2004. doi: 10.3133/ds91.

McCrory, P. A., Blair, J. L., Waldhauser, F., and Oppenheimer, D. H. Juan de Fuca slab geometry and its relation to Wadati-Benioff zone seismicity. *Journal of Geophysical Research: Solid Earth*, 117(B9), Sept. 2012. doi: 10.1029/2012jb009407.

McKenzie, K. A. and Furlong, K. P. Isolating non-subduction-driven tectonic processes in Cascadia. *Geoscience Letters*, 8(1), Mar. 2021. doi: 10.1186/s40562-021-00181-z.

McKenzie, K. A., Furlong, K. P., and Herman, M. W. Bidirectional Loading of the Subduction Interface: Evidence From the Kinematics of Slow Slip Events. *Geochemistry, Geophysics, Geosystems*, 21(9), Sept. 2020. doi: 10.1029/2020gc008918.

Michel, S., Gualandi, A., and Avouac, J.-P. Interseismic Coupling and Slow Slip Events on the Cascadia Megathrust. *Pure and Applied Geophysics*, 176(9):3867–3891, Sept. 2018. doi: 10.1007/s00024-018-1991-x.

Morishige, M. and van Keken, P. E. Along-arc variation in short-term slow slip events caused by 3-D fluid migration in subduction zones. *Journal of Geophysical Research: Solid Earth*, 122(2): 1434–1448, Feb. 2017. doi: 10.1002/2016jb013091.

Mullen, E. K. and Weis, D. Evidence for trench-parallel mantle flow in the northern Cascade Arc from basalt geochemistry. *Earth and Planetary Science Letters*, 414:100–107, Mar. 2015. doi: 10.1016/j.epsl.2015.01.010.

Nishimura, T., Matsuzawa, T., and Obara, K. Detection of short-term slow slip events along the Nankai Trough, southwest Japan, using GNSS data. *Journal of Geophysical Research: Solid Earth*, 118 (6):3112–3125, June 2013. doi: 10.1002/jgrb.50222.

Nuyen, C. P. and Schmidt, D. A. Filling the Gap in Cascadia: The Emergence of Low-Amplitude Long-Term Slow Slip. *Geochemistry, Geophysics, Geosystems*, 22(3), Mar. 2021. doi: 10.1029/2020gc009477.

Okada, Y. Internal deformation due to shear and tensile faults in a half-space. *Bulletin of the Seismological Society of America*, 82 (2):1018–1040, Apr. 1992. doi: 10.1785/bssa0820021018.

Oleskevich, D. A., Hyndman, R. D., and Wang, K. The updip and downdip limits to great subduction earthquakes: Thermal and

structural models of Cascadia, south Alaska, SW Japan, and Chile. *Journal of Geophysical Research: Solid Earth*, 104(B7): 14965–14991, July 1999. doi: 10.1029/1999jb900060.

Ozawa, S. Long-term slow slip events along the Nankai trough subduction zone after the 2011 Tohoku earthquake in Japan. *Earth, Planets and Space*, 69(1), Apr. 2017. doi: 10.1186/s40623-017-0640-4.

Peacock, S. M. The importance of blueschist → eclogite dehydration reactions in subducting oceanic crust. *Geological Society of America Bulletin*, 105(5):684–694, May 1993. doi: 10.1130/0016-7606(1993)105<0684:tiobed>2.3.co;2.

Peacock, S. M. Thermal and metamorphic environment of subduction zone episodic tremor and slip. *Journal of Geophysical Research: Solid Earth*, 114(B8), Aug. 2009. doi: 10.1029/2008jb005978.

Peng, Z. and Gomberg, J. An integrated perspective of the continuum between earthquakes and slow-slip phenomena. *Nature Geoscience*, 3(9):599–607, Aug. 2010. doi: 10.1038/ngeo940.

Plescia, S. M. and Hayes, G. P. Geometric controls on megathrust earthquakes. *Geophysical Journal International*, 222(2): 1270–1282, June 2020. doi: 10.1093/gji/ggaa254.

Plourde, A. P., Bostock, M. G., Audet, P., and Thomas, A. M. Low-frequency earthquakes at the southern Cascadia margin. *Geophysical Research Letters*, 42(12):4849–4855, June 2015. doi: 10.1002/2015gl064363.

Popov, A. A., Sobolev, S. V., and Zoback, M. D. Modeling evolution of the San Andreas Fault system in northern and central California. *Geochemistry, Geophysics, Geosystems*, 13(8), Aug. 2012. doi: 10.1029/2012gc004086.

Rogers, G. and Dragert, H. Episodic Tremor and Slip on the Cascadia Subduction Zone: The Chatter of Silent Slip. *Science*, 300 (5627):1942–1943, June 2003. doi: 10.1126/science.1084783.

Russo, R., VanDecar, J. C., Comte, D., Mocanu, V. I., Gallego, A., and Murdie, R. E. Subduction of the Chile Ridge: Upper mantle structure and flow. *GSA Today*, page 4–10, 2010. doi: 10.1130/gsatg61a.1.

Rüpke, L., Morgan, J., Hort, M., and Connolly, J. Serpentine and the subduction zone water cycle. *Earth and Planetary Science Letters*, 223(1–2):17–34, June 2004. doi: 10.1016/j.epsl.2004.04.018.

Schellart, W. P. Kinematics of subduction and subduction-induced flow in the upper mantle. *Journal of Geophysical Research: Solid Earth*, 109(B7), July 2004. doi: 10.1029/2004jb002970.

Schmalzle, G. M., McCaffrey, R., and Creager, K. C. Central Cascadia subduction zone creep. *Geochemistry, Geophysics, Geosystems*, 15(4):1515–1532, Apr. 2014. doi: 10.1002/2013gc005172.

Schmidt, D. A. and Gao, H. Source parameters and time-dependent slip distributions of slow slip events on the Cascadia subduction zone from 1998 to 2008. *Journal of Geophysical Research: Solid Earth*, 115(B4), Apr. 2010. doi: 10.1029/2008jb006045.

Schwartz, S. Y. and Rokosky, J. M. Slow slip events and seismic tremor at circum-Pacific subduction zones. *Reviews of Geophysics*, 45(3), Aug. 2007. doi: 10.1029/2006rg000208.

Segall, P., Rubin, A. M., Bradley, A. M., and Rice, J. R. Dilatant strengthening as a mechanism for slow slip events. *Journal of Geophysical Research: Solid Earth*, 115(B12), Dec. 2010. doi: 10.1029/2010jb007449.

Shelly, D. R., Beroza, G. C., and Ide, S. Non-volcanic tremor and low-frequency earthquake swarms. *Nature*, 446(7133):305–307, Mar. 2007. doi: 10.1038/nature05666.

Stanciu, A. C. and Humphreys, E. D. Seismic Architecture of the Upper Mantle Underlying California and Nevada. *Journal of Geophysical Research: Solid Earth*, 126(12), Nov. 2021. doi:

10.1029/2021jb021880.

Sweet, J. R., Creager, K. C., Houston, H., and Chestler, S. R. Variations in Cascadia Low-Frequency Earthquake Behavior With Downdip Distance. *Geochemistry, Geophysics, Geosystems*, 20 (2):1202–1217, Feb. 2019. doi: 10.1029/2018gc007998.

Szeliga, W., Melbourne, T. I., Miller, M. M., and Santillan, V. M. Southern Cascadia episodic slow earthquakes. *Geophysical Research Letters*, 31(16), Aug. 2004. doi: 10.1029/2004gl020824.

van Keken, P. E., Hacker, B. R., Syracuse, E. M., and Abers, G. A. Subduction factory: 4. Depth-dependent flux of H2O from subducting slabs worldwide. *Journal of Geophysical Research*, 116(B1), Jan. 2011. doi: 10.1029/2010jb007922.

van Wijk, J. Three-dimensional thermal modeling of the California upper mantle: a slab window vs. stalled slab. *Earth and Planetary Science Letters*, 186(2):175–186, Mar. 2001. doi: 10.1016/s0012-821x(01)00243-6.

Verdonck, D. and Zandt, G. Three-dimensional crustal structure of the Mendocino Triple Junction region from local earthquake travel times. *Journal of Geophysical Research: Solid Earth*, 99 (B12):23843–23858, Dec. 1994. doi: 10.1029/94jb01238.

Wang, K. and Bilek, S. L. Invited review paper: Fault creep caused by subduction of rough seafloor relief. *Tectonophysics*, 610: 1–24, Jan. 2014. doi: 10.1016/j.tecto.2013.11.024.

Wech, A. G. Cataloging Tectonic Tremor Energy Radiation in the Cascadia Subduction Zone. *Journal of Geophysical Research: Solid Earth*, 126(10), Oct. 2021. doi: 10.1029/2021jb022523.

Wech, A. G. and Creager, K. C. A continuum of stress, strength and slip in the Cascadia subduction zone. *Nature Geoscience*, 4(9): 624–628, Aug. 2011. doi: 10.1038/ngeo1215.